Available online at www.sciencedirect.com
SCIENCE DIRECT®
Physica E 29 (2005) 325–333
PHYSICA E
www.elsevier.com/locate/physe

Fano resonances and decoherence in transport through quantum dots

Stefan Rotter[a,*], Ulrich Kuhl[b], Florian Libisch[a], Joachim Burgdörfer[a], Hans-Jürgen Stöckmann[b]

[a]*Institute for Theoretical Physics, Vienna University of Technology, Wiedner Hauptstraße 8-10/136, A-1040 Vienna, Austria*
[b]*Fachbereich Physik, Philipps-Universität Marburg, D-35032 Marburg, Germany*

Available online 7 July 2005

Abstract

A tunable microwave scattering device is presented which allows the controlled variation of Fano line shape parameters in transmission through quantum billiards. We observe a non-monotonic evolution of resonance parameters that is explained in terms of interacting resonances. The dissipation of radiation in the cavity walls leads to decoherence and thus to a modification of the Fano profile. We show that the imaginary part of the complex Fano q-parameter allows to determine the absorption constant of the cavity. Our theoretical results demonstrate further that the two decohering mechanisms, dephasing and dissipation, are equivalent in terms of their effect on the evolution of Fano resonance lineshapes.
© 2005 Elsevier B.V. All rights reserved.

PACS: 05.45.Mt; 73.23.−b; 42.25.−p; 85.35.−p

Keywords: Fano resonances; Decoherence; Ballistic transport; Quantum billiards; Microwave cavities

1. Introduction

Asymmetric Fano line shapes are an ubiquitous feature of resonance scattering when (at least) two different pathways connecting the entrance with the exit channel exist. Fano resonances have been discussed in many different fields of physics starting with photoabsorption in atoms [1–3], electron and neutron scattering [4,5], Raman scattering [6], photoabsorption in quantum well structures [7], scanning tunneling microscopy [8], and ballistic transport through quantum dots (“artificial atoms”) [9–14] and molecules [15,16]. Interest in observing and analyzing Fano profiles is driven by their high sensitivity to the details of the scattering process. For example, since Fano parameters reveal the presence and the nature of different (non) resonant pathways, they can be used to determine the degree of coherence in the

*Corresponding author.
E-mail address: rotter@concord.itp.tuwien.ac.at (S. Rotter).

1386-9477/$ - see front matter © 2005 Elsevier B.V. All rights reserved.
doi:10.1016/j.physe.2005.05.030

scattering device. This is due to the fact that decoherence may convert Fano resonances into the more familiar limiting case of a Breit–Wigner resonance. Furthermore, Fano profiles provide detailed information on the interaction between nearby resonances leading to "avoided crossings" in the complex plane [17,18], and to stabilization of discrete states in the continuum ("resonance trapping" [19,20]). Possible technological applications of Fano resonances have recently been suggested in Ref. [21], exploiting the transmission resonances in transport through open quantum dot systems as a means to generate spin polarization of transmitted carriers.

Using the equivalence between the scalar Helmholtz equation for electromagnetic radiation in cavities with conducting walls and the Schrödinger equation subject to hard-wall boundary conditions [22], we have designed a scattering device (Fig. 1) that allows the controlled tuning of Fano resonances for transport through quantum billiards. The evolution of the Fano parameters as a function of the tuning parameter, in the present case the degree of opening of the leads, can be traced in unprecedented detail, since decoherence due to dissipation can be controlled. By comparison with calculations employing the modular recursive Green's function method (MRGM) [11,23], the parametric variation of Fano resonances and the degree of decoherence can be quantitatively accounted for. Furthermore, the relevant pathways can be unambiguously identified in terms of wavefunctions representing the contributing scattering channels. Due to the equivalence between microwave transport and single-electron motion in two dimensions, our device can be understood as a simulation of ballistic electron scattering through a quantum dot. In contrast to recent investigations of mesoscopic dots and single-electron transistors [9,12,24], where the comparison between theory and experiment has remained on a mostly qualitative level, our model system allows for a detailed quantitative analysis of all features of tunable resonances.

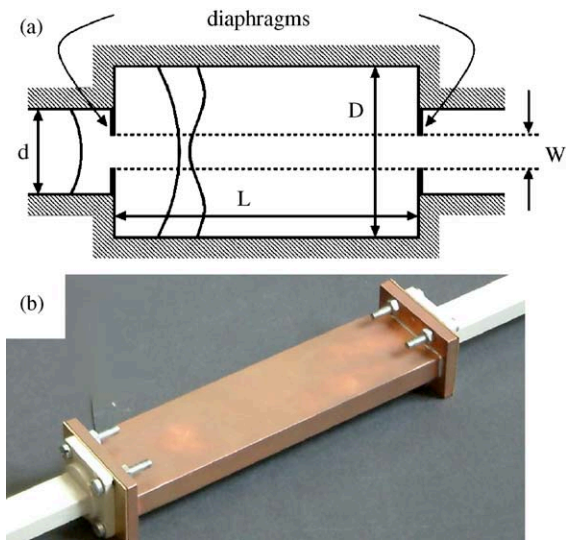

Fig. 1. (a) Schematic sketch of the rectangular cavity with leads attached symmetrically on opposite sides. Exchangeable diaphragms at the lead junctions allow to control the coupling between the cavity and the leads. The open even transverse states are indicated. (b) Photograph of the experimental setup.

2. The model

Our microwave scattering device consists of two commercially available waveguides with height $h = 7.8$ mm, width $d = 15.8$ mm, and length $l = 200$ mm which were attached both to the entrance and the exit side of a rectangular resonator with height $H = 7.8$ mm, width $D = 39$ mm, and length $L = 176$ mm, resulting in a circumference $C = 430$ mm and area $A = 39\,\text{mm} \times 176\,\text{mm}$ (both in the plane). At the junctions to the cavity, metallic diaphragms of different openings were inserted (Fig. 1). The microwaves with frequencies between 12.3 and 18.0 GHz, where two even transverse modes are excited in the cavity and one transverse mode in each of the leads, are coupled into the waveguide via an adaptor to ensure strong coupling.

The experimental results are compared with the predictions of the MRGM. We solve the S matrix for the single particle Schrödinger equation for this "quantum dot" by assuming a constant potential set equal to zero inside and infinitely high outside of a hard-wall boundary. At asymptotic distances, scattering boundary conditions are imposed in the leads. The coupling of the leads to

the cavity of length L can be varied by the two diaphragms which are placed symmetrically at the two lead openings. The lead width d and the width of the rectangular cavity D determine how many flux-carrying modes are open at a certain energy ε in each of the three scattering regions (lead-cavity-lead). We consider in the following the range of wavenumbers where one flux-carrying mode is open in each of the leads. Inside the cavity the first and second even transverse modes are open, thus providing two alternative pathways of transport through the structure. In order to characterize the interfering paths, we decompose the transport across the cavity into a multiple scattering series involving three pieces [25], each of which is characterized by a mode-to-mode transmission (reflection) amplitude or a propagator (see Fig. 2): (1) the transmission of the incoming flux from the left into the cavity, $t^{(\mathrm{L})}$, or reflection back into the lead, $r^{(\mathrm{L})}$, (2) the propagation inside the cavity from the left to the right, $G^{(\mathrm{LR})}$, or from the right to the left, $G^{(\mathrm{RL})}$, and (3) the transmission from the interior of the cavity to the right, $t^{(\mathrm{R})}$, or internal reflection at each of the two vertical cavity walls with amplitude $r^{(\mathrm{R})}$. For the Green's functions (i.e. propagators) $G^{(\mathrm{LR})}(x_{\mathrm{R}}, x_{\mathrm{L}})$ and $G^{(\mathrm{RL})}(x_{\mathrm{L}}, x_{\mathrm{R}})$ we choose a mixed representation which is local in x, and employs a spectral sum over transverse modes, $G^{(\mathrm{LR})}(x_{\mathrm{R}}, x_{\mathrm{L}}) = G^{(\mathrm{RL})}(x_{\mathrm{L}}, x_{\mathrm{R}}) = \sum_n |n\rangle \exp(\mathrm{i}k_n|x_{\mathrm{R}} - x_{\mathrm{L}}|)\langle n|$, where $x_{\mathrm{R,L}}$ are the x-coordinates of the right (left) lead junction with $|x_{\mathrm{R}} - x_{\mathrm{L}}| = L$. The longitudinal momentum for each channel n in the cavity is given by $k_n = \sqrt{k^2 - (k_n^c)^2}$, with the momentum $k = \sqrt{2\varepsilon}$ and the threshold k-values $k_n^c = n\pi/D$. Decoherence due to dissipation of the microwave power in the cavity walls can be easily incorporated by analytically continuing k_n into the complex plane, $k_n = \sqrt{k^2 - (k_n^c)^2} + \mathrm{i}\kappa$.

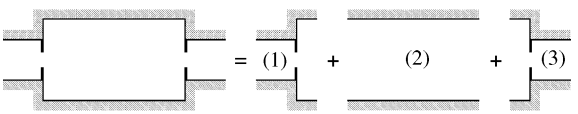

Fig. 2. Decomposition of the scattering device into three separate substructures: (1) a junction from a narrow to a wide constriction (with diaphragm), (2) a wide constriction of length L, and (3) a junction from a wide to a narrow constriction (with diaphragm).

The multiple scattering expansion of the transmission amplitude T is then given by

$$T(k) = t^{(\mathrm{L})} G^{(\mathrm{LR})} \left\{ \sum_{n=0}^{\infty} [r^{(\mathrm{R})} G^{(\mathrm{RL})} r^{(\mathrm{L})} G^{(\mathrm{LR})}]^n \right\} t^{(\mathrm{R})} = t^{(\mathrm{L})} G^{(\mathrm{LR})} [1 - r^{(\mathrm{R})} G^{(\mathrm{RL})} r^{(\mathrm{L})} G^{(\mathrm{LR})}]^{-1} t^{(\mathrm{R})}. \quad (1)$$

The identification of the resonant and non-resonant pathways with help of Eq. (1) is straightforward: due to the absence of inter-channel mixing in the rectangular (i.e. non-chaotic) cavity, the non-resonant contribution corresponds to the $n = 0$ term of the sum describing direct transmission while the resonant contribution is made up by all multiple-bounce contributions ($n \geqslant 1$). The various amplitudes entering Eq. (1) can be parametrized in terms of four phases and two moduli [26]: the modulus, s, of the reflection amplitude of the wave incoming in mode 1 and reflected into mode 1 at the left diaphragm,

$$r_{11}^{(\mathrm{L})} = s\mathrm{e}^{\mathrm{i}\phi_r}, \quad (2)$$

and the modulus, p, of the partial injection amplitude of the incoming wave into the lowest mode of the cavity, corrected for the partially reflected flux (Eq. (2)),

$$t_{11}^{(\mathrm{L})} = t_{11}^{(\mathrm{R})} = p\sqrt{1 - s^2}\ \mathrm{e}^{\mathrm{i}\phi_t^{(1)}}. \quad (3)$$

Because of the symmetry of the scattering device, the injection (ejection) amplitude at the left (right) side are equal. Accordingly, the injection amplitude into the second even mode of the cavity is given by

$$t_{12}^{(\mathrm{L})} = t_{21}^{(\mathrm{R})} = \sqrt{(1 - p^2)(1 - s^2)}\ \mathrm{e}^{\mathrm{i}\phi_t^{(2)}}. \quad (4)$$

Analogous expressions can be deduced [26] for the other partial amplitudes entering Eq. (1). We omit a detailed analysis of the phases in Eqs. (2)–(4) since they do not explicitly enter our analysis in the following. The key observation in the present context is that the square module s^2 is monotonically decreasing between the limiting values $s^2 = 1$ for zero diaphragm opening ($w = 0$) and $s^2 \approx 0$ for fully open diaphragms ($w = d$).

Inserting Eqs. (2)–(4) into Eq. (1), a closed yet complicated expression for the transmission probability $|T(\varepsilon,s)|^2$ as a function of the energy ε and the opening parameter s can be derived [26]. Close to a given resonance $\varepsilon_i^{\mathrm{R}}$ this expression can be approximated by the Fano form [3,26],

$$|T(\varepsilon,s)|^2 \approx \frac{|\varepsilon-\varepsilon_i^{\mathrm{R}}(s)+q_i(s)\Gamma_i(s)/2|^2}{[\varepsilon-\varepsilon_i^{\mathrm{R}}(s)]^2+[\Gamma_i(s)/2]^2}, \tag{5}$$

where $\varepsilon_i^{\mathrm{R}}(s)$ is the position of the ith resonance, $\Gamma_i(s)$ its width, and $q_i(s)$ the complex Fano asymmetry parameter, all of which depend on s. Window resonances appear in the limit $q\to 0$ while the Breit–Wigner limit is reached for $|q|\gg 1$. Since Fano resonances can be identified as resulting from the interference between resonances related to the eigenmodes in the cavity, the parameter q depends very sensitively on the specific position of the involved resonance poles [27,28].

3. Comparison between experiment and theory

In Fig. 3 we present both the experimental and theoretical dependence of the transmission probability $|T|^2$ on k (or ε). In the measurement, the diaphragms were successively closed in steps of 1 mm. The data sets of Fig. 3(a–c) represent the transmission probability for three different values of the opening of the diaphragms $w = 5.8$, 8.8, and 15.8 mm, respectively. Note the remarkable degree of agreement between the measured and the calculated data with only the absorption constant κ as an adjustable parameter. In Fig. 3a where $w/d \approx 0.37$, transport is suppressed and mediated only by resonant scattering with narrow Breit–Wigner shapes centered at the eigenenergies of the closed billiard as indicated by the tick marks. With increasing diaphragm opening (Fig. 3b) transport acquires a significant non-resonant contribution, leading to the widening and the overlap of resonances. Finally, for fully open leads (Fig. 3c), $w/d = 1$ (or $s \approx 0$) resonances appear as narrow window resonances in a non-resonant continuum. The trajectory of the resonance parameter as a function of s can be both experimentally and

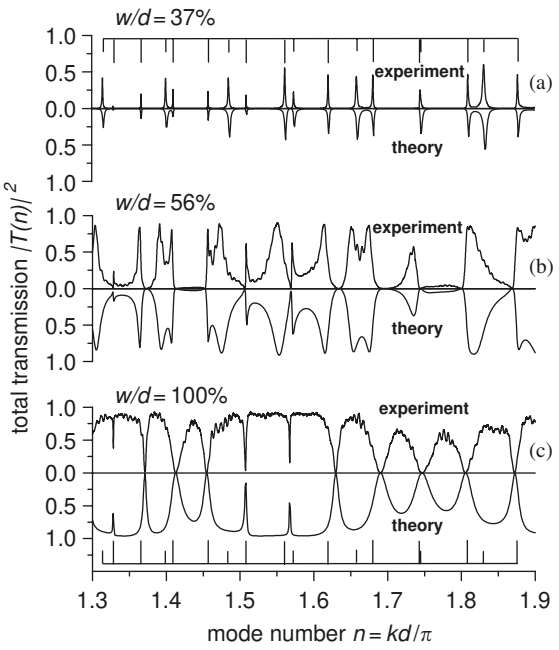

Fig. 3. Total transmission probability, $|T(\sqrt{2\varepsilon}\,d/\pi, w/d)|^2$, for transport through the rectangular cavity with three different openings of the diaphragms: (a) $w/d = 37\%$, (b) $w/d = 56\%$, and (c) $w/d = 100\%$. For better comparison, the experimental and the calculated results are shown as mirror images. The positions of all eigenstates in the closed cavity are indicated by the gray tick marks. For all the calculated curves shown, a damping constant of $\kappa = 10^{-4}\,\mathrm{mm}^{-1}$ was used.

theoretically mapped out in considerable detail. Different types of resonances can be identified by their characteristically different resonance parameters. The evolution of the Fano parameter as a function of w/d (or s) for one resonance is highlighted in Fig. 4. The transition from a narrow Breit–Wigner resonance via a somewhat wider asymmetric Fano profile to a window resonance is clearly observable.

The choice $\kappa = 10^{-4}\,\mathrm{mm}^{-1}$ provides us a good fit and an upper bound of the damping present. Note that even a slightly larger value of $\kappa = 10^{-3}\,\mathrm{mm}^{-1}$ would drastically deteriorate the agreement between experiment and theory (see Fig. 4). In line with the value $\kappa \approx 10^{-4}\,\mathrm{mm}^{-1}$ we obtain an imaginary part of the complex Fano parameter for systems without time-reversal symmetry [24] out of our fitting procedure as $\mathrm{Im}\,q \lesssim 0.1$. We note that by using superconducting

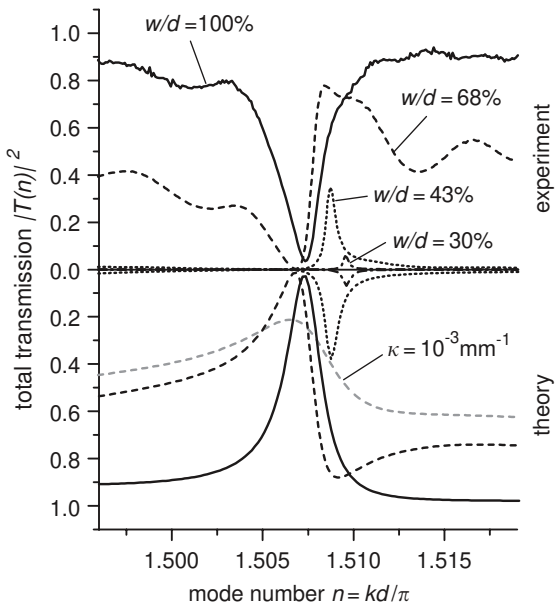

Fig. 4. Fano resonance near the second even excited transverse mode at $kd/\pi \approx 1.5095$. Experimental and theoretical result for four different cavity openings (w/d) are shown. Curves with equal w/d-ratio are displayed in the same line style (solid, dashed, dotted, dash-dotted). For all calculated curves a damping factor $\kappa = 10^{-4}\,\mathrm{mm}^{-1}$ was used, except for the additional gray dashed curve shown for which $\kappa = 10^{-3}\,\mathrm{mm}^{-1}$ and $w/d = 0.68$.

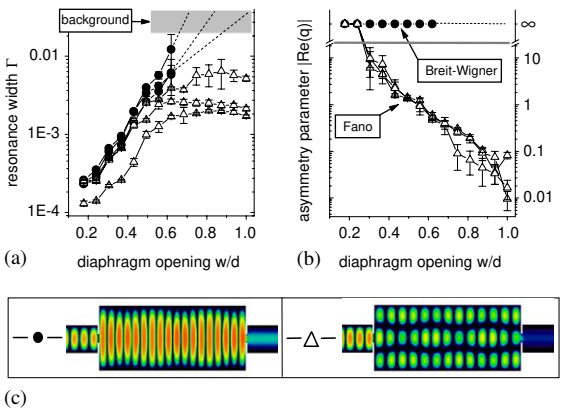

Fig. 5. (a) Resonance width Γ and (b) real part of the asymmetry parameter $|\mathrm{Re}(q)|$ as a function of the diaphragm opening w/d. The data are obtained by fits to experimental results. Solid circles • (empty triangles △) correspond to resonances originating from the first (second) even cavity eigenstate. Typical wavefunctions $|\psi(x,y)|^2$ for these two classes of resonances are shown in (c). In (a) the width Γ of the •-resonances is monotonically growing until resonances disappear in the background of the measured spectra (see gray horizontal bar). For △-resonances Γ reaches a local maximum and slightly decreases for $w/d \to 1$. In (b) the •-resonances always have a $|\mathrm{Re}(q)| > 10$, above which the Fano resonances are very close to the Breit–Wigner lineshape [$\mathrm{Re}(q) = \infty$]. For the △-resonances q shows a strong w/d-dependence: resonances undergo a complete evolution from Breit–Wigner to window type as w/d varies between 0 and 1.

cavities κ could still be further reduced [30], however, with little influence on the result, since we have already nearly reached the fully coherent limit.

4. Evolution of Fano parameters

Following the parametric evolution of a large number of resonances yields a characteristic pattern of Fano resonance parameters (Fig. 5a,b). Obviously, two distinct subsets of resonances appear in the rectangular billiards: one set is characterized by a strictly monotonic increase of Γ with increasing opening of the cavity and a large and only weakly dependent asymmetry parameter q. A second set of resonances features a strongly varying q (on the log-scale!) from large values near the Breit–Wigner limit to values close to $q \approx 0$ for wide opening, yielding a window resonance. At the same time, the width Γ first increases with w/d increasing from close to 0, then reaches a local maximum and finally decreases slightly when $w/d \to 1$. A similar non-monotonic behavior of Γ was recently observed in a single-electron transistor experiment [9]. Such features can be understood in terms of avoided crossings in the complex plane [17,18] between interacting resonances. While the von Neumann–Wigner theorem [31] for bound states predicts avoided crossings between states of the same symmetry and thus a non-monotonic variation of the eigenenergy, interacting resonances can also display avoided crossings on the imaginary axis [17,18], i.e. exchange of the width of resonances and thus leading to a non-monotonic behavior of one of the Γ involved. The two resonance poles approach each other in the complex energy plane and undergo an avoided crossing as a function of the coupling parameter s. As a result, for increasing s

the width of the resonance with large Γ gets even larger and will form a background, on top of which the second narrowed resonance is situated. This somewhat counterintuitive stabilization and narrowing of the width of one resonance despite an increased opening, i.e. an increased coupling to the environment, is sometimes referred to as "resonance trapping" [19,20] and in the limit of $\Gamma \approx 0$ as the "formation of bound states in the continuum". This mechanism could possibly provide an alternative explanation for the results of Ref. [9], where such a non-monotonic behavior was observed and has been previously attributed to increased impurity scattering [24]. A very interesting feature of interacting resonances is the fact that they can be directly related to scattering wavefunctions (see Fig. 5c). Resonances that undergo a complete evolution from a Breit–Wigner to a window resonance are all associated with the *second* even excited state in the cavity, while resonances that display a strictly monotonic increase of the width with increasing cavity opening are connected to transport through the transverse *ground state* of the cavity. This mapping is controlled by the amplitude p for transmission through the first transverse mode (see Eqs. (3) and (4)). In the case that $p^2 > 1/2$ all resonances associated with the first mode are broader than the resonances associated with the excited state and vice versa for $p^2 < 1/2$. For geometric reasons the scattering device studied here (Fig. 1) always favors transport through the first cavity mode and therefore $p^2 > 1/2$. We thus arrive at the remarkably simple result that all resonances associated with the first mode feature a strictly monotonic Γ and a large, but weakly varying q, while all resonances associated with the second mode feature a smaller and non-monotonic Γ with q undergoing the complete evolution from the Breit–Wigner to the window limit. This one-to-one mapping is also indicated in Fig. 3, where only second-mode resonances (indicated by the long tick marks) "survive" the transition of $w/d \to 1$ while all first-mode resonances (short tick marks) vanish in the background of the transmission spectrum. This knowledge could be very useful for the investigation of electron dynamics in mesoscopic scattering systems where the parametric evolution of Fano resonances could yield information about the interaction of internal states and their coupling to the environment.

5. Resonance poles in the complex plane

As discussed above, the transmission amplitudes for scattering through the rectangular cavity can be parametrized in terms of six independent parameters [26] (provided that no dissipation is present). By evaluating the resulting expression for the transmission probability $|T(k_F)|^2$ at complex values of the Fermi wavenumber k_F we can explicitly investigate the resonance poles in the complex plane and their dynamics as a function of the diaphragm opening. Inspired by the work in

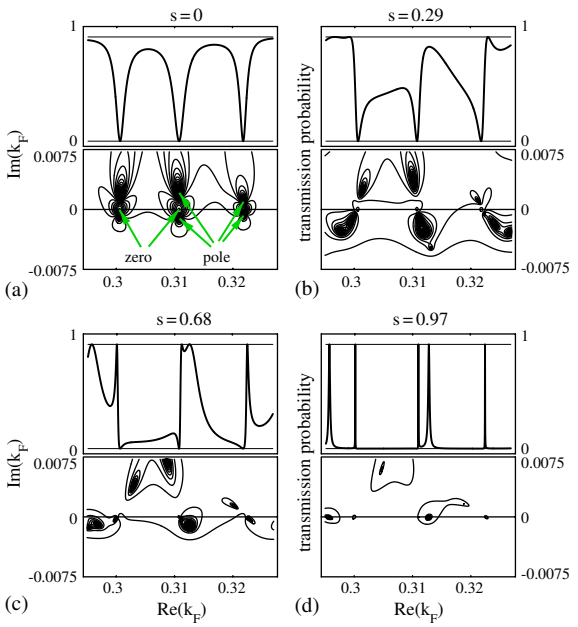

Fig. 6. The calculated k_F-dependence of transmission through the rectangular cavity (without dissipation). The diaphragms are successively closed: (a) $s = 0$, (b) $s = 0.29$, (c) $s = 0.68$, and (d) $s = 0.97$. The upper half of each figure shows the transmission probability $|T(k_F)|^2$ on the real k_F-axis. The lower half depicts contour plots of the transmission probability $|T(k_F)|^2$ in the complex k_F-plane. Poles and zeros in transmission move in the k_F-plane as a function of the opening of the diaphragms. Two of the zeros and four of the poles in (a) are marked by arrows.

Refs. [32,33] we calculated contour plots of the transmission probability $|T(k_F)|^2$ in the complex k_F-plane, displayed in Fig. 6. In general we can associate with every resonance in the transmission probability $|T(k_F)|^2$ a pair of poles for $|T(k_F)|^2$ in the complex k_F-plane and a point on the real k_F-axis where $|T(k_F)|^2$ goes to zero. For full opening of the diaphragms ($s \approx 0$) the complex poles and the points where the transmission probability goes to zero occur at the same Re(k), thus giving rise to almost symmetric resonances (see Fig. 6a). When gradually closing the diaphragms, the poles are situated at a Re(k) which is different from the position of the "zero" on the real axis. Such a configuration gives rise to asymmetric Fano resonances (see Fig. 6b,c). If the diaphragms are almost shut ($s \approx 1$), we are left with poles situated very close to the real k-axis (see Fig. 6d). In line with this observation, the resulting resonances are very narrow and isolated from each other.

6. Decoherence: dephasing versus dissipation

Decoherence in an open quantum system can be caused by different mechanisms: dephasing and dissipation. Both of them are contained in the relaxation operator in a quantum Liouville equation. Decoherence in the microwave scattering device is caused by dissipation, i.e. the absorption of microwave energy by the walls. As discussed above, the absorption constant can be extracted from the shape of the Fano profile in terms of a complex q parameter. The good agreement with theory allows to accurately determine the degree of damping and thus of decoherence present in the experiment. As the Fano profile, in particular near its minimum, is very sensitive to any non-interfering incoherent background, we can determine an upper bound for the damping by comparison between experiment and theory to be $\kappa \lesssim 10^{-4}\,\mathrm{mm}^{-1}$. The consistency of this approach can be checked by an independent calculation of the absorption via the skindepth δ. The cavity in the experiment is made out of oxygen-free copper (DIN 1787:SF-Cu) with a density $\rho \approx 8.9\,\mathrm{kg/dm}^{-3}$ and a conductivity $\sigma \approx 4.9 \times 10^4\,\mathrm{Ohm}^{-1}\,\mathrm{mm}^{-1}$ at room temperature. The skin depth is given by [29]

$$\delta = \frac{1}{\sqrt{\sigma\pi\mu\nu}}, \tag{6}$$

with ν being the microwave frequency and μ the susceptibility of the metal, $\mu \approx \mu_0 = 4\pi 10^{-7}\,\mathrm{Vs}\,(\mathrm{Am})^{-1}$. The quality Q of a resonator is defined as the ratio of the eigenfrequency ν to its width $\Delta\nu$. The Q can be calculated as [29],

$$Q = \frac{\mu}{\mu_0}\frac{H}{\delta}\frac{1}{2 \times (1 + \xi(CH/4A))}, \tag{7}$$

where the height H, the circumference C, and the area A of the cavity enter explicitly. The constant ξ is a geometrical factor close to unity. For the frequency range used in the experiment we find a frequency width $\Delta\nu = \nu/Q \approx 2.5\,\mathrm{MHz}$. Note that this width originates purely in the absorption of microwaves in the cavity walls, as opposed to the resonance broadening caused by the openness of the diaphragms. In line with this result, we find that the above frequency width of 2.5 MHz corresponds very well to the resonance width in the case of small diaphragm opening (i.e. $w/d \lesssim 30\%$), where resonances take on the Breit–Wigner lineshape. The Fourier transform of this resonance form is an exponentially decaying function in coordinate space, the decay constant of which is given by κ. We can therefore directly determine $\kappa = \Delta\nu \times \pi/c$, where c is the speed of light. This finally yields the estimate $\kappa \approx 2.7 \times 10^{-5}\,\mathrm{mm}^{-1}$. The value obtained from the fit of the Fano resonances is somewhat larger ($\kappa \approx 1 \times 10^{-4}\,\mathrm{mm}^{-1}$), which is probably due to additional absorption in the leads.

It has been shown in Ref. [24] that Fano resonances acquire an imaginary q-parameter under the influence of dephasing. Our results presented here clearly indicate that dissipation has the same interference-reducing (i.e. decohering) effect on a Fano resonance as dephasing does. In order to illustrate the equivalence of the decohering effect of dephasing and dissipation on Fano resonances we simulate dephasing in the cavity explicitly and compare with results on dissipative transport. Whereas absorption of microwaves is included in our model by adding

to the real wavenumber in longitudinal direction an imaginary part, $k_n = \sqrt{k^2 - (k_n^c)^2} + i\kappa$, the effect of dephasing is taken into account in the following way: For each of the traversals of the cavity in the multiple scattering expansion of Eq. (1) a Gaussian distributed random phase $\phi_{\rm ran} \in \mathbb{R}$ is added to the longitudinal wavenumbers, $k_n = \sqrt{k^2 - (k_n^c)^2} + \phi_{\rm ran}$ appearing in the constant energy propagators $G^{(\rm LR)}$ and $G^{(\rm RL)}$. The degree of dephasing is controlled by the width of the Gaussian distribution. The numerical data for transmission are then averaged over a large ensemble of different realizations of the random phase.

Note that dephasing, as well as dissipation, causes the unitarity of the scattering process to be violated. Dissipative absorption of microwaves in the cavity walls leads to a net loss of microwave radiation in the system with $U(k) = |T(k)|^2 + |R(k)|^2 < 1$, dephasing causes $U(k)$ to fluctuate *around* the unit value. For a meaningful comparison we enforce unitarity simply by renormalizing the transmission and reflection probabilities explicitly, $|T(k)|^2 \to |T(k)|^2/U(k)$ and $|R(k)|^2 \to |R(k)|^2/U(k)$. We note that rigorous methods for restoring unitarity in open decohering quantum systems are available for both time-independent [24] and time-dependent systems [34]. Fig. 7 illustrates that dephasing and dissipation indeed have a very similar effect on the evolution of Fano resonances and therefore yield complex values of the q-parameter. One conclusion we draw from this finding is that, however useful Fano resonances are as a means to analyze the decoherence present in a scattering process, they do not allow to distinguish between different mechanisms leading to decoherence.

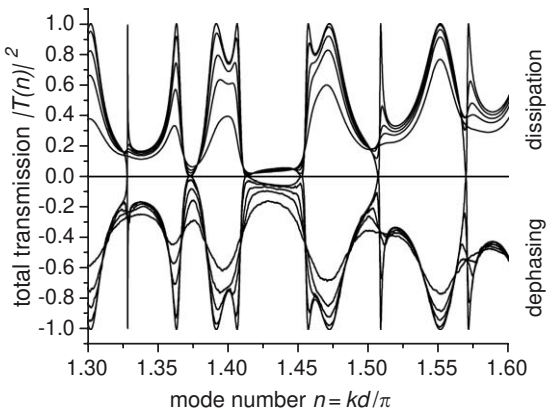

Fig. 7. Renormalized transmission probability, $|T(\sqrt{2\varepsilon}\,d/\pi, w/d)|^2/U(\sqrt{2\varepsilon}\,d/\pi, w/d)$, for transport through the rectangular cavity under the influence of dissipative and dephasing mechanisms, respectively. Opening ratio of the diaphragms $w/d = 56\%$. Above the horizontal axis curves with different dissipation constants κ are shown: $\kappa = 0, 5, 11, 17, 28 \times 10^{-4}\,\mathrm{mm}^{-1}$. The data below the axis contain a random phase factor for each longitudinal crossing of the cavity. The depicted curves feature each a different variance Δk of the Gaussian random phase distribution: $\Delta k = 0, 11, 20, 28, 45 \times 10^{-4}\,\mathrm{mm}^{-4}$. Note that both decohering mechanisms have a very similar effect on the Fano resonances.

7. Summary

In summary, the rectangular microwave cavity attached to two leads allows to study the interplay between resonant and non-resonant transport in unprecedent detail. By a controlled change of the opening, tuning a Fano resonance from the Breit–Wigner limit to the window resonance limit has become possible. Fano resonances can be used to accurately determine the degree of decoherence present in a scattering device. We show that dephasing and dissipative mechanisms have very similar effects on the evolution of Fano resonances. The non-monotonic behavior of resonance parameters can be related to avoided crossings between interacting resonances, which can be unambiguously associated with different resonant modes of the cavity. The latter feature is a consequence of the separability of the wavefunction in the closed cavity. Future investigations along these lines for non-separable chaotic cavities promise new insights into the resonance dynamics of open chaotic systems.

Acknowledgements

We thank D.-H. Kim, K. Kobayashi, C. Müller, E. Persson, I. Rotter, C. Stampfer, and L. Wirtz for helpful discussions. Support by the Austrian

Science Foundation (FWF-SFB016 and FWF-P17359) is gratefully acknowledged.

References

[1] H. Beutler, Z. Physik. 93 (1935) 177.
[2] U. Fano, Nuovo Cimento 12 (1935) 156.
[3] U. Fano, Phys. Rev. 124 (1961) 1866.
[4] R. Adair, C. Bockelman, R.E. Peterson, Phys. Rev. 76 (1949) 308.
[5] J. Simpson, U. Fano, Phys. Rev. Lett. 11 (1963) 158.
[6] F. Cerdeira, T. Fjeldly, M. Carpona, Phys. Rev. B 8 (1973) 4734.
[7] J. Feist, F. Capasso, C. Sirtori, K. West, L. Pfeiffer, Nature 390 (1997) 589.
[8] V. Madhavan, W. Chen, T. Jamneala, M. Crommie, S. Wingreen, Science 280 (1998) 567.
[9] J. Göres, et al., Phys. Rev. B 62 (2000) 2188.
[10] J.U. Nöckel, A.D. Stone, Phys. Rev. B 50 (1994) 17415.
[11] S. Rotter, B. Weingartner, N. Rohringer, J. Burgdörfer, Phys. Rev. B 68 (2003) 165302.
[12] K. Kobayashi, H. Aikawa, S. Katsumoto, Y. Iye, Phys. Rev. Lett. 88 (2002) 256806;
K. Kobayashi, H. Aikawa, S. Katsumoto, Y. Iye, Phys. Rev. B 68 (2003) 235304.
[13] S. Rotter, F. Libisch, J. Burgdörfer, U. Kuhl, H.-J. Stöckmann, Phys. Rev. E 69 (2004) 046208.
[14] B. Weingartner, S. Rotter, J. Burgdörfer, Phys. Rev. B 2005, submitted.
[15] M.L. Ladrón de Guevara, F. Claro, P.A. Orellana, Phys. Rev. B 67 (2003) 195335.
[16] P.R. Levstein, H.M. Pastawski, J.L. D'Amato, J. Phys.: Condens. Matter 2 (1990) 1781.
[17] W.D. Heiss, A.L. Sannino, J. Phys. A 23 (1990) 1167;
W.D. Heiss, A.L. Sannino, Phys. Rev. A 43 (1991) 4159.
[18] J. Burgdörfer, X. Yang, J. Müller, Chaos Solitons Fract. 5 (1995) 1235.
[19] J. Okołowicz, M. Płoszajczak, I. Rotter, Phys. Rep. 374 (2003) 271 and references therein.
[20] E. Persson, I. Rotter, H.-J. Stöckmann, M. Barth, Phys. Rev. Lett. 85 (2000) 2478.
[21] J.F. Song, Y. Ochiai, J.P. Bird, Appl. Phys. Lett. 82 (2003) 4561.
[22] H.-J. Stöckmann, Quantum Chaos: An Introduction, Cambridge University Press, Cambridge, 1999.
[23] S. Rotter, J.-Z. Tang, L. Wirtz, J. Trost, J. Burgdörfer, Phys. Rev. B 62 (2000) 1950.
[24] A.A. Clerk, X. Waintal, P.W. Brouwer, Phys. Rev. Lett. 86 (2001) 4636.
[25] L. Wirtz, C. Stampfer, S. Rotter, J. Burgdörfer, Phys. Rev. E 67 (2003) 16206.
[26] D.-H. Kim, H.-S. Sim, K.J. Chang, Phys. Rev. B 64 (2001) 115409;
D.-H. Kim, H.-S. Sim, K.J. Chang, Phys. Rev. B 67 (2003) 129903 (E).
[27] H.-W. Lee, Phys. Rev. Lett. 82 (1999) 2358.
[28] A.I. Magunov, I. Rotter, S.I. Strakhova, Phys. Rev. B 68 (2003) 245305.
[29] J.D. Jackson, Classical Electrodynamics, Wiley, New York, 1999.
[30] A. Richter, in: D.A. Hejhal, et al. (Eds.), Emerging Applications of Number Theory, The IMA Volumes in Mathematics and its Applications, vol. 109, Springer, New York, 1999, p. 479.
[31] J. von Neumann, E. Wigner, Phys. Z. 30 (1929) 467.
[32] W. Porod, Z. Shao, C.S. Lent, Phys. Rev. B 48 (1993) R8495.
[33] Z. Shao, W. Porod, C.S. Lent, Phys. Rev. B 49 (1994) 7453.
[34] M. Seliger, et al., Nucl. Instr. and Meth. B 230 (2005) 7;
M. Seliger, et al., Phys. Rev. A, 2004, accepted for publication.